Chapter 4

Abel inversion

Abel inversion is a technique used in several fields, for instance in Astronomy to derive the radial mass distribution of a galaxy using the observation of its emitted light. In a ionospheric context it is possible to apply this inversion on the STEC data observed by GPS onboard LEO satellites in order to obtain the electron density expressed in function of height. Abel inversion is a direct and straightforward technique, which make it very appealing to process GPS data sensitive to vertical structures of electron density (for instance data gathered by GPS receivers onboard LEOs).

4.1 Inversion Techniques

Two types of GPS observations can be used to apply the Abel inversion:

1. *Bending angle*. The presence of a refractivity index in the different layers of the atmosphere causes a bending in the electromagnetic signal. This refractivity index depends on pressure, humidity and temperature for the neutral atmospheric layers and on the electron density in the case of ionosphere. The bending effect is more important in the lower parts of the atmosphere, therefore it is mainly used for tropospheric profiling. In the case of the ionosphere, although the signal is still affected by the bending, its effect is less important. The advantages of this observable is that its noise level is low. Nevertheless, this technique requires either precise orbits and clocks of both GPS and LEO, to accurately model the range from L1 or LC (ionospheric free combination) observations.

2. With the *STEC* information contained in the L_I observable it is possible to directly derive the electron content of the ionosphere. The advantage is that with this observable the clock and orbit errors are removed.

4.1.1 Inverting from bending angle data

The method of inverting occultation data using bending angle can be summarized in two steps that will be detailed in this section:

1. To obtain the bending angle from the observations (based on the scheme depicted in Figure 4.1)

2. To establish a link between the bending angle and the refraction index. At this point, the Abel transform will be needed to invert this relationship and obtain the refractivity index profile. Afterwards the vertical profiles of electron density are directly obtained from this inverted profile.

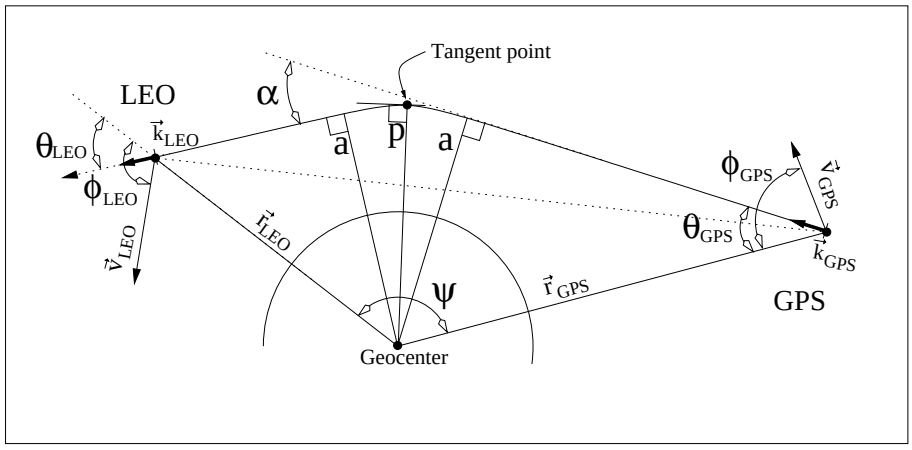

Figure 4.1: Scheme of occultation geometry

Computing the bending angle

Analyzing the geometry involved in an occultation (see Figure 4.1) and using the fact that the sum of all inner angles of a quadrilateral is always 2π, one can obtain the expression of the bending angle (α):

$$\alpha = \theta_{LEO} + \theta_{GPS} + \psi - \pi \tag{4.1}$$

With this equation by itself it is not possible to obtain the bending angle. An additional equation is given by the extra Doppler shift. This GPS data observable is expressed, as it is well known, in function of the radial velocity between the emitter (i.e. LEO satellite) and the transmitter (i.e. GPS satellite):

$$D = -\frac{f_e}{c} v_\rho \tag{4.2}$$

where f_e is the nominal transmitted frequency, c is the speed of light in the vacuum and v_ρ is the radial velocity. Therefore, inspecting the geometry involved in an occultation (see Figure 4.1), one can obtain an equation that will allow to solve for the angles θ_{LEO} and θ_{GPS}, and therefore α: let $\vec{k}_{GPS}$ and $\vec{v}_{GPS}$ be the unit vectors of the ray at the GPS location and velocity vector of the GPS respectively (and similarly $\vec{k}_{LEO}$ and $\vec{v}_{LEO}$ for the LEO satellite), therefore, the Doppler shift can be expressed in the following way:

$$D = \frac{f_e}{c}(\vec{v}_{GPS} \cdot \vec{k}_{GPS} - \vec{v}_{LEO} \cdot \vec{k}_{LEO}) \tag{4.3}$$

Therefore, based on the notation of angles showed in Figure 4.1, this expression yields to:

$$D = \frac{f_e}{c}(v_{GPS}\ \cos(\phi_{GPS} - \theta_{GPS}) - v_{LEO}\ \cos(\phi_{LEO} - \theta_{LEO})) \tag{4.4}$$

An important point that allows to solve for the angles required to obtain the bending angle is the assumption of spherical symmetry, that through the *Bouguer's formula* (equivalent to Snell's law in a spherically symmetric medium, see [Born and Wolf, 1975]) states that:

$$n_{GPS}\ r_{GPS}\ \sin\theta_{GPS} = n_{LEO}\ r_{LEO}\ \sin\theta_{LEO} = a = constant \tag{4.5}$$

In this expression it is commonly assumed that either n_{LEO} and n_{GPS} (index of refraction at the location of the LEO and GPS respectively) is 1. According to [Hajj and Romans, 1998], this assumption causes an overestimation of the electron density of no more than 0.5%.

The angles ϕ_{GPS} and ϕ_{LEO} can be directly found using the dot product of the velocity and position vectors of the GPS and LEO satellites.

Afterwards, the angles θ_{GPS} and θ_{LEO} are obtained using the previous relationships, thus allowing to solve for the bending angle α.

Inverting the bending angle data with Abel transform

The assumption of spherical symmetry allows to set out a relationship between the bending angle (α) and the index of refraction (n), using the Bouguer's formula. Since the impact parameter a is constant in the straight

line, it is possible to compute the bending angle (which is the departure of the true ray from the ideal assumption of a straight line). Therefore:

$$\begin{array}{lcl} \text{Straight Line} & \Rightarrow & r\ \sin(\theta_s) = a_s \\ \text{True ray (Bouguer's formula)} & \Rightarrow & n\ r\ \sin(\theta) = a \end{array} \tag{4.6}$$

Differentiating both expressions, multiplying the straight line one by the refraction index and subtracting both equations it is obtained the following:

$$dn\ r\ \sin\theta + n\ dr\ (\sin\theta - \sin\theta_s) + n\ r\ (\cos\theta\ d\theta - \cos\theta_s\ d\theta_s) = 0 \tag{4.7}$$

Since the bending angle at the ionospheric heights, specially from the F layer, does not exceed 0.03^o even during daytime and near solar maximum ([Hajj and Romans, 1998],[Schreiner et al., 1999]), it is possible to approximate the previous expression to:

$$dn\ r\ \sin\theta + n\ r\ \cos\theta(d\theta - d\theta_s) = 0 \tag{4.8}$$

The differential of the bending angle $d\alpha$ is, in fact, the quantity $d\theta - d\theta_s$, therefore recalling the Bouguer's formula, the previous expression yields to:

$$d\alpha = -\frac{\sin\theta}{\cos\theta}\frac{dn}{n} = -\frac{\sin\theta}{\cos\theta}d\ln(n) = -\frac{a}{\sqrt{x^2 - a^2}}d\ln(n) \tag{4.9}$$

where $x = n\ r$. The bending angle α is obtained integrating the previous expression for the path towards the GPS and the path towards the LEO, that is:

$$\alpha(a) = -a\left[\int_a^{x_{GPS}} + \int_a^{x_{LEO}}\right]\frac{1}{\sqrt{x^2 - a^2}}\frac{d\ln(n)}{dx}dx \tag{4.10}$$

Assuming that above the LEO the contribution the the bending angle is negligible and taking advantage of the symmetry of both paths (due to geometric symmetry and the assumption of spherical symmetry), the final expression for the bending angle is obtained:

$$\alpha(a) = -2\ a\int_a^{\infty}\frac{1}{\sqrt{x^2 - a^2}}\frac{d\ln(n)}{dx}dx \tag{4.11}$$

Note that the assumption of spherical symmetry implies that the refractivity index depends only on height. Applying the Abel integral transform on this expression ([Tricomi, 1985]), it is possible to obtain the index of refraction in function of the impact parameter a:

$$ln(n(x)) = \frac{1}{\pi}\int_x^\infty \frac{\alpha(a)}{\sqrt{a^2 - x^2}} da \tag{4.12}$$

The index of refraction provides with the electron density since

$$n = 1 - 40.3 \times \frac{N_e}{f^2} \tag{4.13}$$

where the minus sign is related to the use of phase (i.e. phase advance), N_e is the electron density expressed in $electrons/m^3$ and f is the frequency of the signal expressed in $Hertz$. This expression is, in fact, an approximation quite good for the occultation retrieval purpose. Those terms non included in the expression (third and larger order terms) are several orders of magnitude smaller ([Hardy et al., 1993]). In fact, the errors due to the inversion process are much larger than these neglected terms ([Schreiner et al., 1999]).

4.1.2 Inverting from STEC data

The inversion using STEC data is based on the fact that the bending angle due to ionosphere is very small, specially for the layer F2 of the ionosphere and upwards, and the separation of the different paths of the L1 and L2 frequencies is less than 3km ([Hajj and Romans, 1998]). This assumption of small bending angle can cause a certain mismodelling in the E layer, but this is usually masked by the assumption of spherical symmetry. Under these assumptions, the ray between the LEO and the GPS can be modeled as a straight line as shown in Figure 4.2.

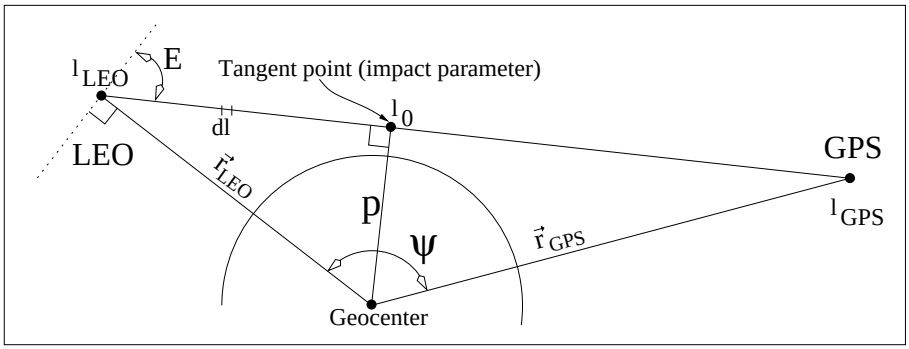

Figure 4.2: Scheme of occultation geometry with straight line

Therefore the tangent point (impact parameter p) can be assumed to be equal since the bending angle is neglected. The value of its height can be expressed as:

$$r_{tangent\ point} = p = r_{LEO} \cdot \sin(90 + E) = r_{LEO} \cdot \cos E \tag{4.14}$$

where h_{LEO} is the height of the LEO satellite and E is the elevation of the LEO satellite with respect to the GPS satellite (E is positive for observations above the LEO and negative for observations underneath, as in the case of Figure 4.2).

Based on the definition of the STEC as the line integral of the electron density (see Equation 1.23), and with the assumption of spherical symmetry (i.e. the Electron density N_e only depends on height h) it is possible to express the STEC as the Abel transform of the electron density:

$$\begin{aligned} STEC(p) &= \left[\int_{l_0}^{l_{LEO}} + \int_{l_0}^{l_{GPS}}\right] N_e(r)dl = {}^{[l=\sqrt{r^2-p^2} \Rightarrow dl=\frac{r}{\sqrt{r^2-p^2}}dr]} \\ &= \left[\int_{l_0}^{l_{LEO}} + \int_{l_0}^{l_{GPS}}\right] \frac{N_e(r)r}{\sqrt{r^2-p^2}}dr = {}^{(*)}\ 2\int_{l_0}^{l_{LEO}} \frac{N_e(r)r}{\sqrt{r^2-p^2}}dr = \\ &= \mathcal{A}[N_e(r)] \end{aligned} \tag{4.15}$$

The step marked with an asterisk ($^{(*)}$) can be done assuming that the electron content above the LEO is neglected and considering the geometric symmetry of the problem, thus reducing the two integrals in one. This formulism of the Abel inversion corresponds to the case introduced in [Bracewell, 2000], which yields to the following result:

$$N_e(r) = -\frac{1}{\pi}\int_r^{r_{LEO}} \frac{dSTEC(p)/dp}{\sqrt{p^2-r^2}}dp \tag{4.16}$$

In the case of the GPS data, the analysis of the ionospheric combination (P_I or L_I) implies that the STEC is affected by a bias containing the instrumental biases and phase ambiguity (in the case of L_I), therefore care must be taken in order to account for these terms. Moreover, the result obtained in these sections make two important assumptions that are one of the main topics of this work: (1) the treatment of the electron content above the LEO orbit and (2) the overcoming of the spherical symmetry limitations.

Recursive inversion of STEC data

The recursive scheme of the Abel inversion starts with the STEC discretisation, that can be expressed, neglecting the discretisation errors, as:

$$STEC(n) \simeq 2 \cdot \sum_{i=1}^{n} N_e(p_i) \cdot l_{i,n} \tag{4.17}$$

Each STEC observation defines a layer in the vertical profile, therefore, the sampling rate at which the LEO gathers GPS data will determine the vertical resolution of the profile (for instance one sampling each second (1Hz) yields to a vertical resolutions of units of km).

Starting with the uppermost observation (that one with the highest impact parameter p) and processing downwards assuming the same hypothesis assumed in the previous approaches of Abel inversion, the electron density can be obtained as follows:

$$N_e(p_n) = \frac{STEC(n) - 2 \cdot \sum_{i=1}^{n-1} N_e(p_i) \cdot l_{i,n}}{2 \cdot l_{n,n}} \tag{4.18}$$

An schematic view of this algorithm is depicted in Figure 4.3. Note that the spherical symmetry implies that the electron density within the same layer is constant. Nevertheless, as it will be shown in further sections, an occultation may cover wide areas in which this hypothesis is not clearly fulfilled, causing a mismodelling.

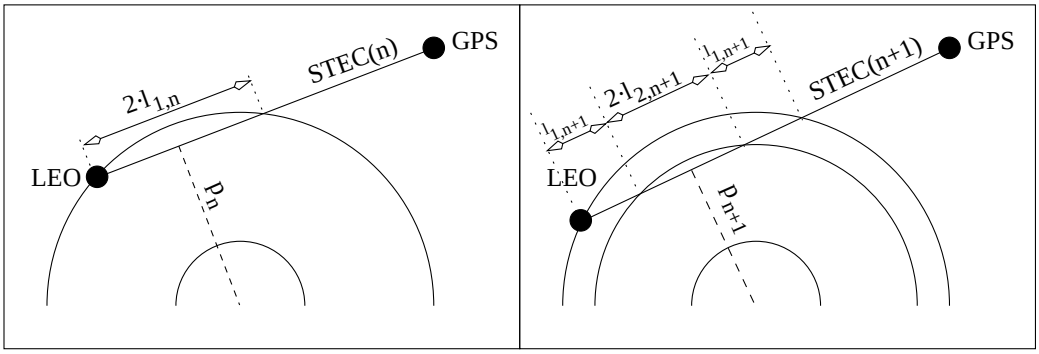

Figure 4.3: Scheme of discrete inversion of STEC

4.2 LEO GPS missions

In the recent years, several missions consisting on LEOs that carry GPS receivers among other instruments allow the scientific community to broadly apply the Abel inversion. Moreover, this data can be used in the ionospheric tomography algorithms as well, in order to improve the vertical resolution compared with the methods that use ground data alone.

In this context the GPS/MET mission was the first one to carry a GPS receiver, thus allowing to perform the proof of concept of the Abel inversion

applied to GPS data. The GPS/MET satellite (launched in April 3, 1995 and decommissioned in March 1997) had a circular orbit at 730 km of altitude and 60 degree of inclination.

Currently, there are more LEOs with a GPS receiver onboard such as the recent missions SAC-C and CHAMP. SAC-C satellite (acronym of *Satélite de Aplicaciones Científicas*) carries onboard the GOLPE instrument (GPS Occultation and Passive Reflection Experiment) devoted to gather data from radio occultations. The orbit of this satellite is approximately circular, and it is placed at 702km of height with 98.2 degrees of inclination. A concurrent mission to SAC-C is the CHAMP satellite (CHAllenging Minisatellite Payload). The nominal initial orbit of this satellite is placed at 454km with 87 degrees of inclination. Nevertheless, due to the atmospheric drag, the altitude of CHAMP will decrease to the expected value of 300km by the end of its lifetime (5 years). There is an important difference with respect to the GPS/MET mission regarding the Solar cycle. During the GPS/MET lifetime, the Solar cycle was at a minimum. On the contrary, these two latter missions take place during a period of maximum in the Solar cycle, thus making it more difficult to estimate the profiles as will be seen in a following chapter.

The CHAMP satellite presents a feature that makes it a challenge in the application of the Abel inversion. As said before, one of the approximations of the Abel technique is that the electron content above the LEO is neglected. For LEOs at high altitudes such as GPS/MET and SAC-C an exponential extrapolation can be enough to account for the contribution of the upper ionosphere and plasmasphere above the LEO (applied to bending angle data in [Hajj and Romans, 1998] and applied in the vertical profile in [Hernandez-Pajares et al., 2000]). Nevertheless this approximation causes a mismodelling for LEOs with very low orbit such as CHAMP, which can even be under the hmF2 height in certain periods. Therefore a more accurate modeling of the upper ionosphere and plasmasphere is needed.

In the future it is planned the launch of the COSMIC LEO constellation. This constellation consists in 6 satellites distributed in 3 orbital planes spaced 60 degrees. The nominal height of each satellite will be 700km with 72 degrees of inclination. This constellation, in conjunction with additional concurrent missions, will multiply the possibilities of the ionospheric sounding based on GPS data gathered by either ground and LEO satellites.

More details and data on these missions can be found at the following web servers:

1. JPL-Genesis web server: *http://genesis.jpl.nasa.gov/*
2. SAC-C web page: *http://www.conae.gov.ar/satelites/sac-c.html*

3. CHAMP web page at GeoForschungsZentrum: *http://op.gfz-potsdam.de /champ/*

4. COSMIC web at UCAR: *http://www.cosmic.ucar.edu/*

4.2.1 Expected performance

Several possibilities exist to evaluate the performance of the inverted profiles. If a controlled environment is needed (for instance to test the proof of concept of the algorithm) it is possible to rely in a simulated scenario. With the IRI model, for instance, it is possible to simulate the STEC seen by the LEO using the actual geometry of the occultation (that is, using the real orbits of the satellites). Afterwards this observable is inverted and the electron density profile is obtained. The resulting values of the electron density can be compared with those provided by the model.

Since the ionosphere presents irregularities and features that are not included in climatological models and due to the presence of instrumental delays and cycle slips (only in the phase) in the GPS observations, the scenarios with real data are harsher. In this type of scenarios, the plasma measurements carried on by ionosondes (in particular the foF2 parameter) are the usual validation performed to evaluate the performance of the inverted profiles. With the spherical symmetry assumption, it is expected that the discrepancies with respect to the ionosonde measurements of foF2 are comprised from 10% to 20% (which corresponds to discrepancies of 20% to 40% respectively in electron density NmF2, see for instance [Hajj and Romans, 1998], [Schreiner et al., 1999] or [Hajj et al., 2000]). There are several factors that affect these performances:

1. The presence of non-constant horizontal gradients of electron density causes a mismodelling in the spherical symmetry assumption. Two particular cases of this points are the Equatorial anomalies, that mainly affect the occultations that take place at low latitudes during daytime, and the day/night terminators (dusk and dawn periods) where the gradients induced by the rapid changes of the Sun radiation cause a failure in the spherical symmetry assumption.

2. The co-location, which is not present for the case of simulated comparisons. This source of error is mainly due to the spatial and temporal mismatch between ionosonde and occultation. In the case of simulated data with a model it is possible to obtain the electron density values for each desired location and time, but in the case of ionosonde, the soundings are made to a certain locations at a limited epochs.

Part II

Results on algorithms for 3D ionospheric sounding

Chapter 5

Combining Ionosonde and ground GPS data

5.1 Complementarity of data

As mentioned in previous sections, GPS data gathered by ground receivers (opposed to receivers on-board LEO satellites) are basically insensitive to the vertical distribution of the ionospheric electron content. This is due to the geometry involved in the ground GPS observations, which is mainly vertical, thus incrementing the difficulty to distinguish the contribution of each layer in the vertical, causing strong correlations between the corresponding estimates. Therefore, an additional complementary data source is needed to decorrelate the layers in the vertical. In this context, [Hernandez-Pajares et al., 1998] described the use of both ground and LEO GPS data to perform 3D ionospheric imaging. To quantify the goodness of the method, direct measurements of ionospheric plasma frequencies (see Section 1.4.1) given by ionosondes were used for comparison. Following the idea of combining different data, this chapter is focused on mixing ground GPS and ionosonde data with the objective to provide with an alternative solution to the 3D description of the electron content ([Garcia-Fernandez et al., 2002],[Garcia-Fernandez et al., 2003c]).

With the ionospheric parameters obtained from ionosonde measurements it is possible to obtain vertical profiles up to the maximum of electron density applying algorithms such as POLAN ([Titheridge, 1998]) or even up to higher altitudes by extrapolating up to higher altitudes using models such as NeQuick ([Hochegger et al., 2000]) or IRI ([Bilitza, 1990],[Bilitza, 2001]). Therefore, the vertical information provided by these data sources can complement the ground GPS data in the task of giving vertical description of the ionosphere up to the hmF2.

The effect of including vertical information (in this case from ionosonde data) can be seen in Figure 5.1, where it is plotted the profile before and after considering ionosonde information. Using ground GPS alone, one can expect to obtain non realistic profiles that can even take negative values. The integration of the different cells in height provides with correct values of VTEC, but it is not possible to decompose properly its integral into the

different values of electron density in the vertical. On the contrary, when vertical information is added to the method (for instance from a background model or from ionosonde), it is possible to decorrelate these layers and to obtain more realistic profiles. In this example, the objective was the estimation of the vertical profile of electron density over the ionosonde of *Slough* (E0.6 N51.5) at 10hUT, but considering (constraining) information coming from a different ionosonde, in this case from the ionosonde of *El Arenosillo* (E6.73 N37.1).

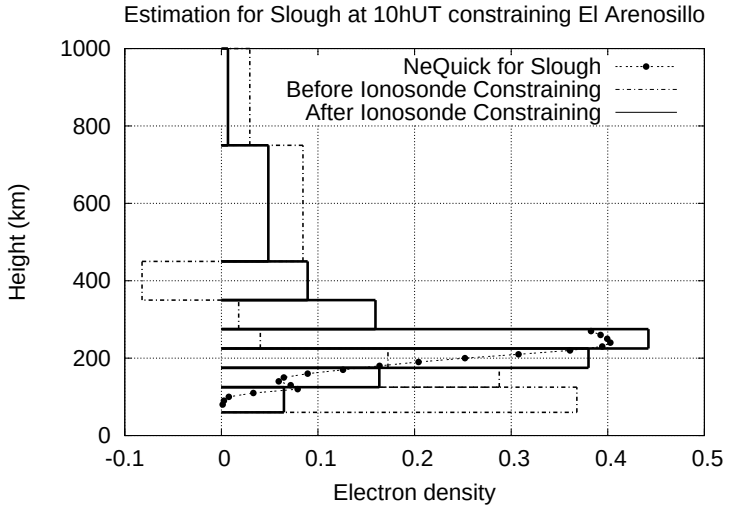

Figure 5.1: Vertical description of electron density obtained before and after using ionosonde profiles

The results presented in this chapter show that the combination proposed causes the GPS data to expand in longitude/latitude the vertical resolution provided by the ionosonde data, and to expand in height the horizontal resolution provided by the ground GPS data, as predicted using simulated data in [Hernandez-Pajares et al., 1999].

5.2 Model

Ionospheric modeling

Section 3.2.1 explained the state-of-the-art regarding the modeling of the ionosphere in a tomographic context. The approach used in this work divides the ionosphere in a set of cells or volume elements (i.e. voxels). Therefore, the resulting estimates of the algorithm are the electron densities in each of

these cells. These values are assumed to be constant in each cell and during the time span processed.

The size of cells is greatly influenced by the fact that the electron density is assumed to be constant in each cell. As said in Section 3.2.1, this size must follow a compromise; they must be large enough to allow that at least few rays traverse them and to keep the computational load low (i.e. less unknowns to solve), but if the size is too large, the estimated values of electron density will not reflect the actual variations inside the cells (similar effect occurs in image processing when an image is digitized using too large pixels). This last point can be specially critical when large variations of electron density take place, for instance in low latitudes (near the geomagnetic equator), during ionospheric storms or in high geomagnetic conditions. Since the data set used in this work corresponds to the year 1995, a period of low solar activity, and the area of study is mid-latitude, the size of the cells have been set to $7.5^o \times 5^o$ in LT and latitude respectively as done in [Hernandez-Pajares et al., 1999]. Table 5.1 shows figures of relative variations within a shell in different conditions using a climatological model, in this case the IRI. With this table in mind it is clear that the cell size should be reconsidered when processing data sets that include low-latitude regions or high solar activity periods.

		Cell Size	
		$7.5^o \times 5^o$	$15^o \times 10^o$
Mid-latitude 2E45N	Solar minimum 1995 290 13hUT (13hLT)	9%	20%
Low-latitude 120E22N	Solar maximum 2000 201 6hUT (14hUT)	23%	36%

Table 5.1: Relative variation of electron density within a typical cell of 50km of width in height, from 200km to 250km. The percentual value refers to the relative variation of the electron density within a cell with respect to its average value. This table has been obtained using the IRI model. The extreme case corresponds to the low latitude regions in maximum of solar cycle, as expected, which shows the largest variations. The location of the cell center in longitude and latitude as well as the epoch in year, day of year and hour in UT and LT are also given.

With respect to the distribution in height, the program accept as an input the layer centers, which have been set to the following heights: 100km, 150km, 200km, 250km, 300km, 400km, 500km and 1000km. Upper and lower boundaries of the ionosphere are considered to be 60km and 2000km

respectively. The boundaries of each layer are afterwards computed as the mid-point between centers. With this approach, the layers are polyhedrons rather than volumes divided by spheres in height. For the cell size considered in this work, the differences in geometry considering spherical boundaries and plane boundaries do not exceed 15km in the worst case, being 0km in the grid points. Figure 5.2 shows the distributions of the borders. With this division in height the vertical variability of the ionospheric electron density is accounted for. The layer centers, and therefore its corresponding boundaries, are chosen based on geometric considerations (i.e. they must be large enough in height), that is on how the process is able to distinguish between layers using the available data. Besides the geometry of data, the number of height layers are limited by computer load as well.

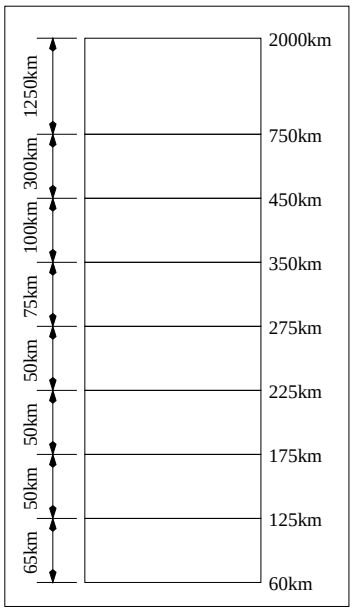

Figure 5.2: Vertical layers considered for the method of mixing complementary data. The left hand side shows the height width of each layer and the right hand side the boundaries of each vertical layer, which are the mid-distance between centers. In this work the centers have been set to: 100km, 150km, 200km, 250km, 300km, 400km, 500km and 1000km.

The inverse problem

The GPS observable used in this work to obtain the estimation of the electron densities is the ionospheric (geometric free) combination of phases (see Section 2.2.1). This choice is due to the fact that the phase observables are

much more precise than the code observations of the ionospheric combination (phase observables errors are in the level of millimeters while the associated errors of the code ones is around meter or larger and strongly affected by multipath).

The errors due to multipath, wind-up and noise are much more small than the ionospheric effect. Thus, the relationship between the ionosphere and the ionospheric combination of phases derived from the GPS observables can be expressed as ([Hernandez-Pajares et al., 1999], [Hernandez-Pajares et al., 2000]).

$$L_I = \alpha \cdot STEC + b_I \tag{5.1}$$

where $\alpha = 1.0506[meters\ of\ delay \cdot m^2/10^{17} electron]$ and b_I contains the instrumental delays and phase ambiguity. Assuming a straight line propagation between the GPS satellite transmitter and the GPS receiver and a ionosphere divided in voxels (in which each voxel is identified by the local time index (LT_i), latitude index (ϕ_j) and height index (h_k)) the integral of the STEC (see Equation 1.23) can be discretised and rewritten as:

$$STEC = \sum_i \sum_j \sum_k N_e(LT_i, \phi_j, h_k) \cdot l(LT_i, \phi_j, h_k) \cdot \delta(LT_i, \phi_j, h_k) \tag{5.2}$$

where $N_e(LT_i, \phi_j, h_k)$ is the electron density in cell (LT_i, ϕ_j, h_k) at the observation time, l is the length of the ray portion and δ is equal to 1 if the ray "illuminates" the (LT_i, ϕ_j, h_k) cell and 0 otherwise (see Figure 5.3 for a schematic view).

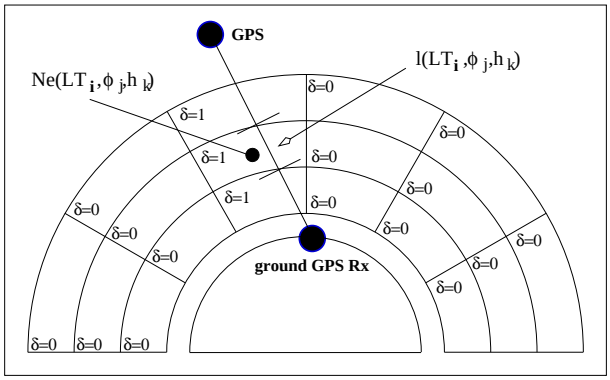

Figure 5.3: Scheme of STEC modelisation in a ionosphere divided in voxels

In this system, the direct problem (reconstruction of L_I) can be solved provided that the electron densities and biases are known. Nevertheless, the measurements are the phase observations of the ionospheric combination

L_I, therefore, the inverse problem needs to be solved in order to obtain the electron densities and biases.

The first step then is to set out the equations based on GPS following the Equations 5.1 and 5.2, and to obtain a solution based only on ground GPS data. The resulting estimates of electron density are highly correlated as expected (see Figure 5.1). To solve this, ground GPS data is reprocessed with the aid of data from ionosondes. To compute the solution of data combination, a Gauss Markov model with equality constraints ([Koch, 1988]) is considered. This approach is similar to those based on Weighted Least Mean Squares in which the constraints would be considered as observations with very higher weight than the ordinary observations.

To orientate the solution obtained with ground GPS data, the electron density profiles derived from NeQuick, anchored previously to ionosonde measurements, are used to build the constraints. An schematic view of how they are constructed is summarized in Figure 5.4. Since the ionosphere is modeled with 8 layers and the NeQuick vertical profiles can offer resolutions of 10km, the first step is to average the profiles in the vertical dimension according to the distribution in height indicated in Figure 5.2 (so an averaged value of the electron density $\hat{N}_e$ is obtained). The resulting values are applied to the nearest grid center with respect to the constrained ionosonde.

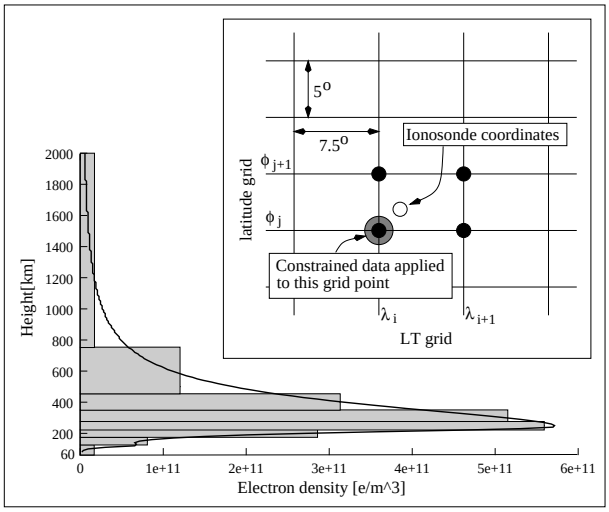

Figure 5.4: Construction of constraints from Vertical profiles derived from ionosonde data

This produces equality constraints on specific cells. The constraining scheme is based on two types of conditions, which are:

1. Under hmF2, values of averaged vertical profiles of ionosondes are used

to built equality constraints of the form:

$$N_e(LT_i, \phi_j, h_k) = \hat{N}_{e,NeQuick}(LT_i, \phi_j, h_k) \quad for \quad h_k < h_m F_2 \tag{5.3}$$

2. Above hmF2, ratios between values from the NeQuick electron density values, anchored to bottomside ionosonde measurements, are used to fix a relationship in height between densities. Therefore, these constraints are built from the following relationship:

$$\frac{N_e(LT_i, \phi_j, h_k)}{N_e(LT_i, \phi_j, h_{k+1})} = \frac{\hat{N}_{e,NeQuick}(LT_i, \phi_j, h_k)}{\hat{N}_{e,NeQuick}(LT_i, \phi_j, h_{k+1})} \quad for \quad h_k > h_m F_2 \tag{5.4}$$

The choice of dividing the constraining scheme in two groups of constraints is because up to hmF2 the models are computed anchoring NeQuick to direct ionosonde measurements. The values for the topside ionosphere are obtained, in the case of NeQuick, from a semi-Epstein function, which follows a climatological behavior in terms of the top-sounding data used to elaborate NeQuick. Therefore, ratios between height layers are considered instead of direct values to take into account a certain model for the upper layers of the ionosphere.

The data are processed each 3 hours using a Sun fixed reference frame (the ionosphere is divided in LT and latitude). Since the Sun is the main source of ionisation in the ionosphere, it is possible to assume that the electron content is constant in this period (due to the relative stationarity of the chosen reference frame). If the ionosphere were divided in longitude and latitude (i.e. Earth fixed reference frame), assuming the electron density constant in each cell would introduce an important mismodelling due to the Earth rotation. This rotation gives the system dynamics, thus allowing the ground GPS receivers and ionosondes to "illuminate" successive cells. Thus, this approach is possible in front of more elaborated techniques such as adaptive or Kalman filtering, applied in other scenarios such as in [Sardon et al., 1994] or [Hernandez-Pajares et al., 1998].

5.3 Results

Since phase data has been considered for this work, all GPS phase observables has been given in a noise level of 0.1TECU (1cm of error). The formal

errors obtained show typical values of $0.1e10e/m^3$, which provide an RMS of approximately 1TECU in the residual (i.e. observation minus calculus). Nevertheless, the formal errors may be realistic only to a limited extent and only useful to discard those estimates with large errors (outliers) and to see correlations between estimations.

Formal errors will depend, among other factors, on the noise level of the measurements and the relative weights assigned to each of the data types considered in the process. The validation proposed to assess the performance of the model, relies basically on the comparison with independent data in order to provide with a more complete evaluation of the error.

In this context, and based on the data type used to quantify the error in the estimates, two comparisons are proposed: (1) with ionosonde profiles that has not been taken part into the process (i.e. electron density comparison) and (2) with observations gathered by LEO satellites with a GPS receiver on-board (i.e. STEC comparison).

5.3.1 Scenario

The study of this work has been carried out using real data from ground GPS receivers and ionosondes of Europe (see map in figure 5.5 and distances between ionosondes in table 5.2).

	El Arenosillo	Juliusruh	Moskow	Rostov
Slough	1673	995	2496	2918
Rostov	3924	2003	937	
Moskow	3860	1518		
Juliusruh	2475			

Table 5.2: Table of distances between ionosondes in kilometers

The days of study are 1995 October 17th, 18th and 19th. Although this period corresponds to Solar Minimum conditions, the Dst parameter, plotted in figure 5.6, shows the presence of a ionospheric storm. In the same figure (lower panel), the VTEC corresponding to different European stations indicates that this storm affected the central-north European regions (in particular the ionosondes of *Slough* and *Juliusruh-Ruegen*).

5.3.2 Comparison with Ionosonde data

The estimates of electron densities are obtained using ground GPS data and NeQuick vertical profiles derived from one or two (at most) ionosondes (i.e.

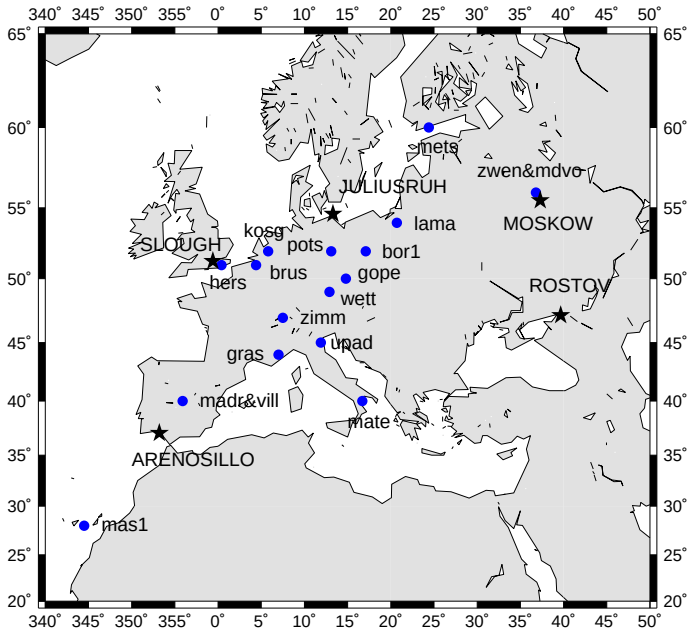

Figure 5.5: Map of IGS European GPS stations and ionosondes used for this scenario

constrained ionosondes). Afterwards, these estimates are compared with the other unused NeQuick vertical profiles (i.e. test ionosondes). Note that the vertical resolution obtained with the proposed method is limited to 8 shells (with 50km as the smallest resolution) and the NeQuick vertical profiles offers resolutions of 10km. Therefore, the NeQuick profiles used to compare are averaged according to the distribution of layers indicated previously. The resulting densities are compared with the estimations. Figure 5.7 shows two examples of cases of performance with the RMS, computed as the difference between values of electron densities at different heights. Additionally, the errors regarding the estimation of the NmF2 (relative error) are also given.

The resulting comparison between the estimated profiles and those provided by NeQuick are summarized in Table 5.3. The table gives the RMS (in units of $10^{10}e^{-}/m^{3}$) of the difference between the complete profiles up to the maximum. Moreover, the performance with respect to the estimation of the NmF2 is given as well. It presents different situations, for low and high geomagnetic activity and with different ionosondes constrained. In parentheses the number of comparisons made for each case (all points of the profile for the RMS comparison and only the maximum for the NmF2).

Since the thickness of the lower shells is approximately 50km, the reso-

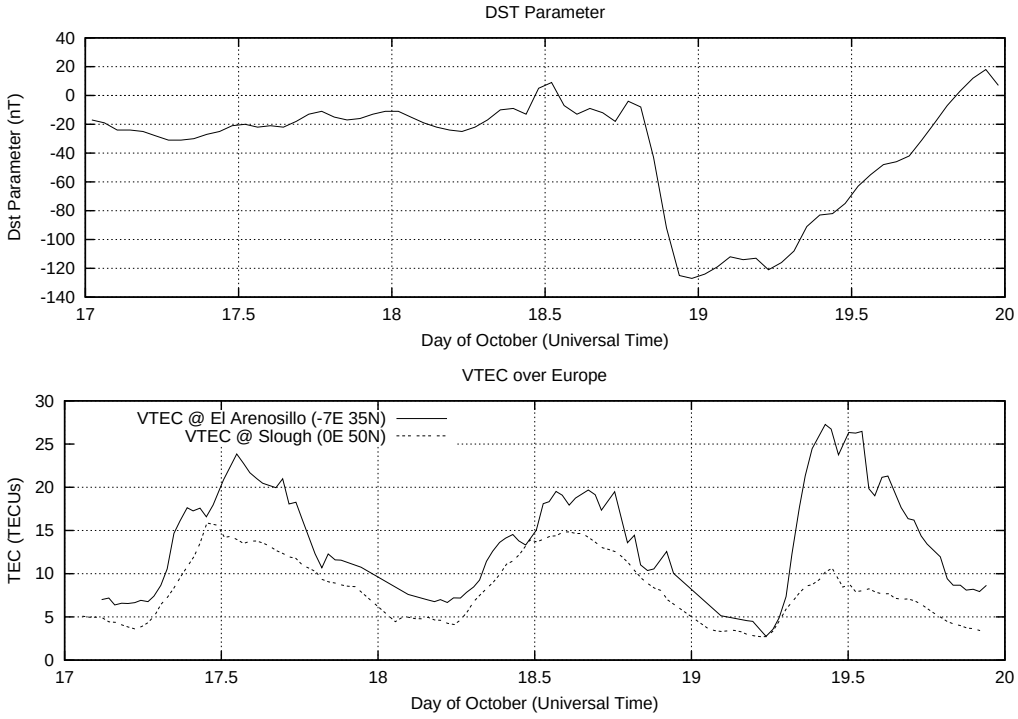

Figure 5.6: Dst parameter during 1995 October 17th, 18th and 19th

lution in height of this method is limited to 25km, thus introducing a corresponding additional source of error in such comparison. An additional mismodelling is introduced due to the limited resolution of 8 layers, causing that only averaged electron densities can be compared. Note as well that although the electron density estimations can have relatively low errors, a shift in height can have large effects in the overall RMS of the profiles. An example of this effect can be seen in Figure 5.7, where the comparison for *Juliusruh/Ruegen* shows a displacement of the profile in height and, therefore, the resulting profile RMS is larger than the other case, where there is no shift in height.

The table is divided according to the geomagnetic activity and the number of ionosondes constrained (marked with an asterisk). The geomagnetic activity is considered to be low if the Dst parameter is above -40nT and high if below this point. The ionospheric storm mentioned above lasted beyond October 20th, therefore the data set only contains the beginning of the storm, but not its complete evolution.

The constrained ionosondes (at the West side of the network) are selected in order to diminish the spatial-temporal correlation between these and the test ionosondes (i.e. the ones used for comparative purposes). Supposing

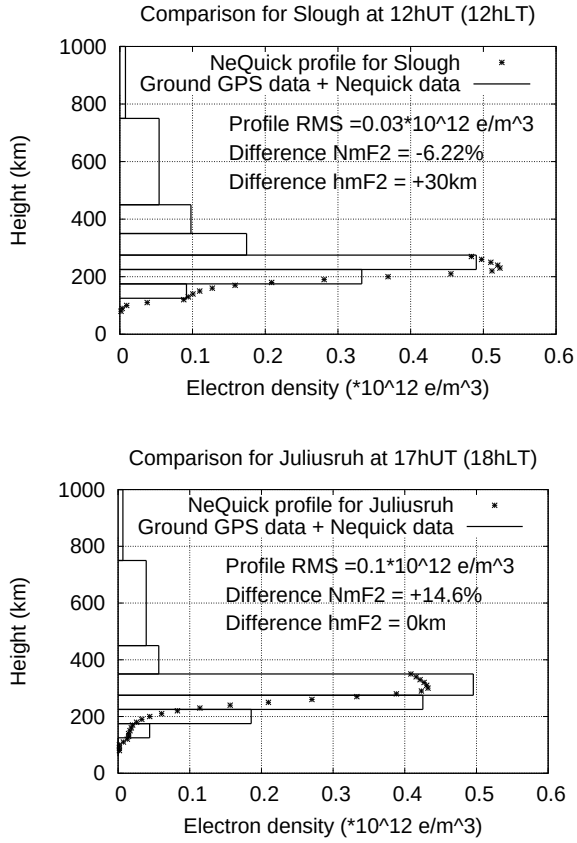

Figure 5.7: Examples of profile estimation using ground GPS and Ionosonde data. Statistics for each profile are also shown

that *Moskow* ionosonde would be chosen instead, since the process is done in a Sun fixed reference frame and due to the Earth rotation, the past sounding of this ionosonde would directly inform about the ionosphere above the ionosondes of *Juliusruh* and *Slough*, which are 1.5h and 2.5h of difference in LT (see map in Figure 5.5), thus increasing the spatial-temporal correlations between ionosondes. Based on this criterion, *El Arenosillo* ionosonde has been selected to test this strategy in a bad case scenario. The differences in the estimation of the maximum are of the same order than other methods such as the Abel inversion (see Chapter 4). Looking at the results obtained in low and high geomagnetic activity it can be seen that the errors are larger in the latter case. This is due to the fact that the storm affected in a different way the central and northern ionosondes with respect to those located in southern Europe as indicates the depletion of the VTEC over the

	low geomagnetic activity		high geomagnetic activity	
	Profile RMS $10^{10}e^-/m^3$	Diff. NmF2 %	Profile RMS $10^{10}e^-/m^3$	Diff. NmF2 %
Arenosillo *	4 (112)	-15.5 (24)	6 (107)	-22.7 (19)
Juliusruh	6 (104)	-18.6 (19)	19 (85)	139.2 (13)
Moskow	8 (116)	-6.4 (21)	15 (70)	-9.1 (8)
Rostov	7 (68)	-23.8 (12)	16 (56)	77.1 (6)
Slough	5 (88)	-4.7 (13)	25 (42)	103.3 (8)
Arenosillo *	4 (111)	-11.2 (24)	6 (107)	-27.7 (19)
Juliusruh *	1 (97)	-10.0 (18)	2 (84)	-25.6 (13)
Moskow	6 (102)	15.8 (18)	5 (67)	-54.0 (8)
Rostov	5 (56)	-5.4 (9)	9 (56)	-29.0 (6)
Slough	4 (84)	-0.3 (13)	5 (42)	5.7 (8)

Table 5.3: Comparative between the computed electron density profiles with respect to those provided by the NeQuick model derived from ionosonde measurements. The first 5 rows correspond to the case of one ionosonde constrained, and the last 5 to the case with 2 ionosondes constrained. The asterisk mark the constrained ionosondes. In parenthesis the number of comparisons, note than in the case of the profile RMS, since all of the bottomside points are compared, the number of comparisons is larger.

northern ionosonde (shown in the lower panel of figure 5.6). Note that *El Arenosillo* shows different patterns of VTEC compared with northernmost ionosondes such as *Slough*. This fact is reflected in the table, where the error of considering only 1 ionosonde is greater than if an additional ionosonde were introduced, specially during the storm. If a second ionosonde affected by the storm is constrained, the estimation of the profile is improved. This is specially true during high geomagnetic activity, where the information provided by this additional ionosonde is shown to be valuable to decrease the error on the estimation due to the effect of the storm, in spite of not using Kalman filter.

Table 5.3 shows a lack of 100% agreement in the estimation of the constrained ionosondes for the whole profile, which is due to the interpolation effect. The estimation is performed in a regular grid, therefore to obtain the vertical profiles over a ionosonde location it is necessary to interpolate between the 4 nearest grid centers. The coordinates of *Juliusruh* are close to one of the grid centers, therefore the values of the grid in the vertical are directly the constraining ones and the remaining grid center contributions are smaller, thus the interpolation error is small. In the case of *El Arenosillo*, it

is placed equidistant to the nearest 4 grid centers, thus the constraint over this station can not be seen in the reconstruction due to the effect of the interpolation. Notice that the values obtained from a constrained ionosonde are applied to the nearest grid center. Table 5.3 shows that this interpolation error may vary from the lower value of $1e10e/m^3$ corresponding to the case of *Juliusruh*, to the worst case, that corresponds to the *El Arenosillo* ionosonde, in which this value reaches $4e10e/m^3$. During high geomagnetic periods, the interpolation error may be increased. If the regular grid is completed with centers placed at ionosonde locations, the estimations of the constrained ionosondes improves, but there are no substantial improvement on the estimated ionosondes and, besides, it increases the needed computer memory and processing time.

Regarding the performance in the hmF2 parameter, the maximums where detected in the same vertical cell that would correspond to the profiles of the test ionosondes. As mentioned before the best vertical resolution by the bottomside is 25km, so it can be considered that the uncertainty error for the hmF2 estimation of the model is 25km in average.

An additional result can be seen in figure 5.8, a 1 to 1 comparison between the estimated and NeQuick values for the NmF2. Since *Slough* is inside the area limited by *El Arenosillo* and *Juliusruh*, its estimation errors are less when compared with other ionosondes that are outside this area, this is the case of *Rostov-on-Don*

5.3.3 Comparison with GPS LEO data

An additional comparison can be carried out considering the observations gathered by LEOs with a GPS receiver on-board, which consisted in dual frequency codes and phases. For this scenario, all available ionosonde information was used to obtain the electron density estimates (i.e. all ionosondes are constrained) and the STEC observations gathered by this satellite were used for comparative purposes.

Once the electron densities have been computed, and using the geometry of the GPSMET satellite, the direct problem (Equation 5.2) is applied in order to reconstruct the STEC (see also Figure 5.9 for a schematic view).

Using the actual measurement of the LEO satellite, an additional source of comparison is obtained. This type of data is quite sensitive, as in the case of ionosonde, to the vertical distribution of the ionospheric free electron. Once the STEC is reconstructed, it is compared with the actual measurements of the GPSMET. Note that GPSMET observations provide with the L_I observable, but not with the STEC directly. Nevertheless, following equation 5.1, it can be seen that the L_I is basically the STEC plus a bias (errors

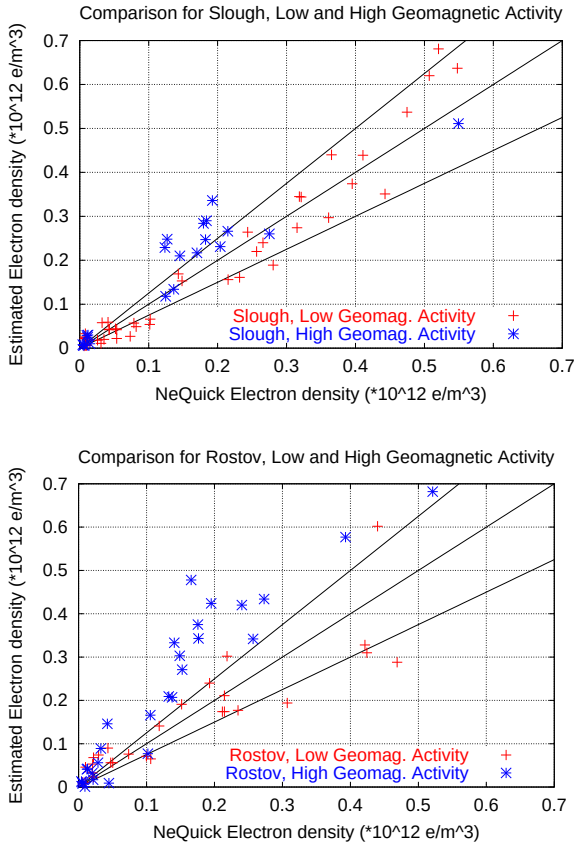

Figure 5.8: Estimated value of NmF2 against the one provided by NeQuick (anchored by ionosonde value of NmF2). Middle line is 100% agreement, side lines are ±25% of error boundary.

due to multipath and wind-up are regarded as noise measurements in this work). In order to compare the same magnitudes (i.e. reconstructed STEC with measured STEC and not measured L_I), for a given occultation, the L_I observation with higher tangent point (where the STEC is expected to be lowest) is subtracted from the rest L_I observations. Figure 5.10 gives a comparison of an occultation made up of 54 STEC observations against the height of the tangent point , both the reconstructed STEC and the STEC observed by the GPSMET are shown. The peak region corresponds to those STEC observations affected by the NmF2. Since there are a large amount of these kind of observations, it is possible to check the performance of this method in these regions.

A 1 to 1 plot summarizing this type of comparison is shown in figure 5.11.

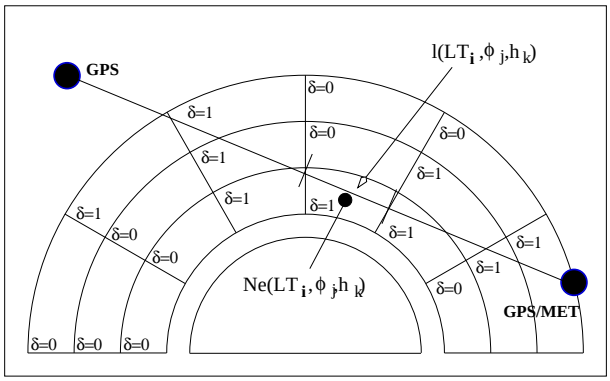

Figure 5.9: Scheme of STEC Reconstruction for a LEO observation in a ionosphere divided in voxels.

The figure plots the Reconstructed STEC (using the estimates of the electron density) in the y-axis and the observed STEC values of the GPSMET in the x-axis. This plot shows that there are more agreement for the reconstructions under hmF2 since the resolution given to these layers are lower than for the upper ones. Moreover, the constraints are build from a model anchored with ionosonde measurements (better constraints). This sum of factors leads to this result. This point can be seen as well in figure 5.10, where the estimated STEC above the peak maximum shows a coarser behavior compared with the observations under the peak. The average error in the estimation of the STEC is better than 25% under the hmF2.

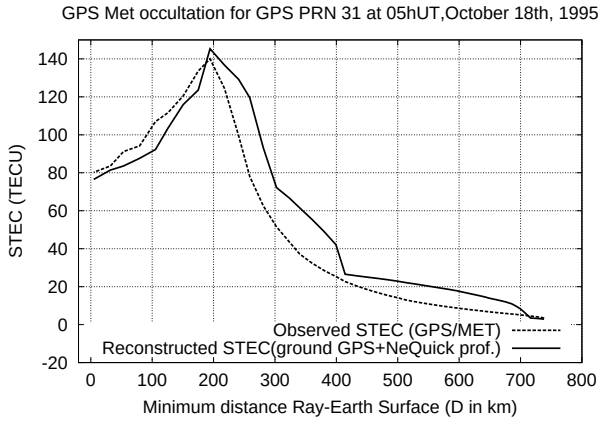

Figure 5.10: Example of a single occultation comparison. STEC (expressed in TECU) against the minimum distance between the ray and earth surface (height of tangent point).

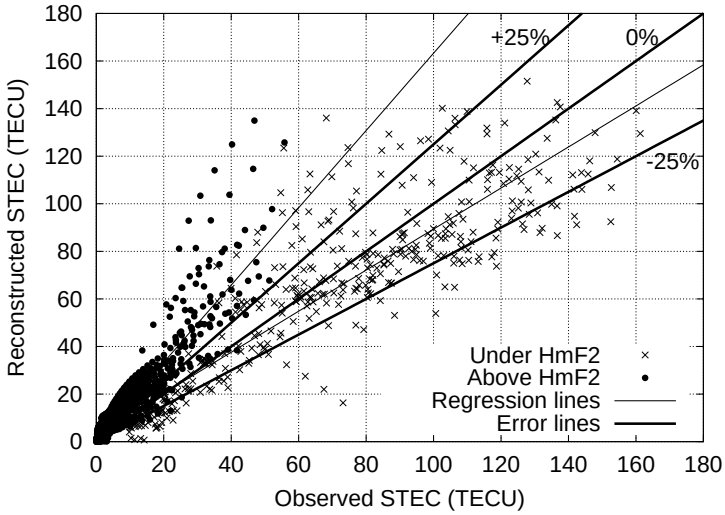

Figure 5.11: General overview of occultation comparison. Points correspond to the STEC observed during 1995 October 18th, 30 occultations and 1641 points have been compared. The regression lines corresponding to both cases are also depicted.